Formation and Evolution of a Freshwater Plume in the Northwestern Tropical Atlantic in February 2020

Gilles Reverdin, Léa Olivier, G. Foltz, Sabrina Speich, J. Karstensen, J. Horstmann, D. Zhang, R. Laxenaire, Xavier Carton, Hubert Branger, et al.

A freshwater plume in the northwestern tropical Atlantic in February 2020

Reverdin, G.[1], L. Olivier[1], G. R. Foltz[2], S. Speich[3], J. Karstensen[4], J. Horstmann[5], D. Zhang[6], R. Laxenaire[7], X. Carton[8], H. Branger[9], R. Carrasco[5], J. Boutin[1]

[1]LOCEAN-IPSL, Sorbonne Université-CNRS-IRD-MNHN, Paris, France, Paris, France

[2]NOAA/Atlantic Oceanographic and Meteorological Laboratory, Miami, FL, USA,

[3]Laboratoire de Météorologie Dynamique, ENS-Ecole Polytechnique-CNRS-Sorbonne Université, Paris, France.

[4]GEOMAR Helmholtz Centre for Ocean Research Kiel, Kiel, Germany

[5]Helmholtz-Zentrum Geesthacht, Geesthacht, Germany

[6]CICOES/University of Washington and NOAA/Pacific Marine Environmental Laboratory, Seattle, WA, USA

[7]Center for Ocean-Atmospheric Prediction Studies, Florida State University, Tallahassee, Florida, USA.

[8]Laboratoire d'Océanographie Physique et Spatiale, UBO-CNRS-IFREMER-IRD, Plouzané, France.

[9]IRPHE, CNRS-AMU, Luminy, France.

Corresponding author: Gilles Reverdin (gilles.reverdin@locean.ipsl.fr)

Key Points:

- Very stratified fresh water plume separates from Guiana shelf in early February 2020, carrying northward 0.15 Sv during 10 days.
- After 14 days, the plume reaches an extent of 100000 km^2, with minimum surface salinity eroding from 30 pss to 33.3 pss.
- Plume probably initiated by wind direction shift closer to the equator, 5-7 days earlier and stirred by a North Brazil Current ring.

Abstract

In February 2020, a 120km-wide freshwater plume was documented by satellite and in situ observations near the Demerara Rise (7°N/54-56°W). It was initially stratified in the upper 10 m with a freshwater content of 2 to 3 meters of Amazon water distributed down to 40 m. On February 2nd, ship transects indicate an inhomogeneous shelf structure with a propagating front in its midst, whereas minimum salinity close to 30 pss was observed close to the shelf break on February 5th. The salinity minimum eroded in time but was still observed 13 to 16 days later with 33.3 pss minimum value up to 400 km from the shelf break. At this time, the mixed layer depth was close to 20 m. The off-shelf flow lasted 10 days, contributing to a plume area extending over 100000 km^2 and associated with a 0.15 10^6 m^3 s^{-1} freshwater transport. The off-shelf plume was steered northward by a North Brazil Current ring up to 12°N and then extended westward toward the Caribbean Sea. Its occurrence follows 3 days of favourable wind direction closer to the Amazon estuary, which contributed to north-westward freshwater transport on the shelf. Other such events of freshwater transport in January-March are documented since 2010 in salinity satellite products in 7 out of 10 years, and in 6 of those years, they are preceded by a change in wind direction between the Amazon estuary and the Guianas that is favorable for north-westward freshwater transport toward the shelf break.

Plain language summary

This paper documents how freshwater from the Amazon reaches the deep ocean up to 12°N in the northwest tropical Atlantic in January-March. The classical view is that the water is channelled along the shelf to the Caribbean Sea. Here, we document a freshwater plume from in situ and satellite observations during the EUREC4A-OA/ATOMIC program. This plume separated from the shelf near 55°W north of French Guiana on February 2-5. This fresher water was stirred by a North Brazil Current ring up to 12°N before mostly spreading westward. The near-surface water is initially very stratified at least until 10-m from the surface. More than 14 days later and 400 km farther north, salinity as low as 33.3 pss with mixing depths on the order of only 20-m was still encountered. The total area of the freshwater plume reached 100000 km^2 with a flow of freshwater on the order of 0.15 10^6 m^3 s^{-1} during 10 days. This phenomenon seems to be triggered by changes in the wind direction on the shelf closer to the equator, and has also been observed in 7 out of 10 years since 2010.

1. Introduction

The main topics of this paper are the freshwater transport from the Guiana shelves offshore to the Northwest tropical Atlantic in boreal winter and the processes that control this transport. Fresher surface layers are often relatively thin and induce a strong stratification in the upper ocean layers limiting the turbulent heat and momentum fluxes across the base of the mixed layer. This condition has the potential to enhance near-surface cooling by sensible and latent surface heat fluxes and the trapping of momentum enabling the development of barrier layers and temperature inversions at the base of the halocline (Mignot et al, 2012). Freshwater originating from the shelves can also carry nutrients and organic matter that sustain food webs.

The freshwater input by the Amazon and other northeastern South American rivers is minimal in December and progressively increases from January to May. During this period, the North Brazil Current (NBC) retroflection is either non-existent or weak. As a consequence, January through March is the season of maximum salinity in the northwestern tropical Atlantic west of 45°W, with no offshore transport of freshwater at the NBC retroflection, and with salty water flowing over the Guiana shelves and continental slope. In January-March, according to Fournier et al. (2017), the freshwater plume extension (defined by salinity less than 35.5 pss) is minimal north of South America. However, even in this season, occasional freshwater transport from the shelves, either induced by eddies or the winds (via the Ekman transport), might lead to the development of surface freshened layers (Mignot et al, 2012).

Satellite surface imagery (L-band radiometry) illustrates that this off-shore freshwater transport does not happen frequently in January (Fig 1a, 1b), but it is often present in

February (Fig. 1c, d) and later in the year. In February, the weekly sea surface salinity (SSS) product (http://dx.doi.org/10.5285/4ce685bff631459fb2a30faa699f3fc5) used here for 2010-2019 shows a band of maximum variability near the shelf break between 54°W and 58°W and peaking near 55°W. Though the maximum is within 100 km of the shelf break, the increase in variability compared to January extends all the way to 12°N in the longitude range 54.5°W-58°W, and it is associated with intermittent fresh plumes. This seems to lower the average surface salinity in this offshore region.

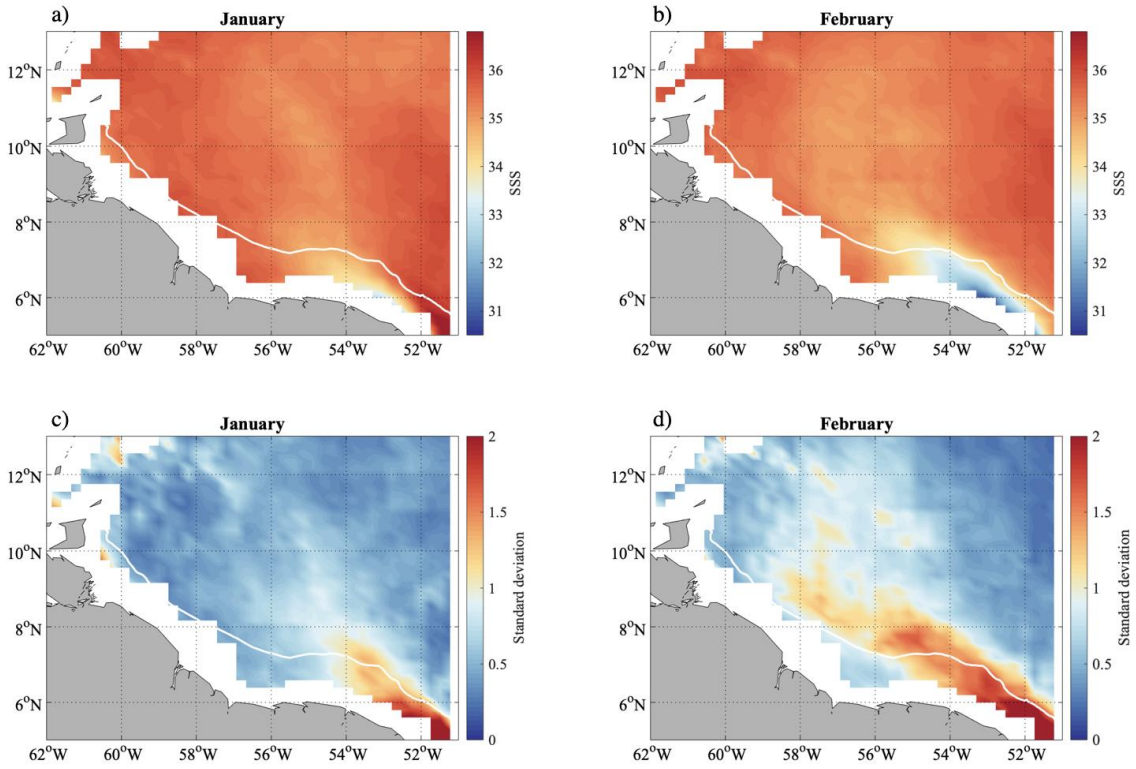

Figure 1: Average salinity and its standard deviation based on weekly CCI SSS products in 2010-2019. Upper panels: averages for January and February, and lower panels the corresponding standard deviations.

Pathways of surface freshened layers originating from the shelves and ultimately from the Amazon have been followed in the past using satellite ocean colour imagery (Müller-Karger et al, 1988; Hu et al, 2004) and more recently the L-band microwave imagery of surface

salinity (Salisbury et al, 2011; Grodsky et al, 2014; Fournier et al, 2015, 2017). Quantification of advection and transport of surface fresh water in such analyses is hindered in two ways. On one hand, colour imagery is not a direct estimate of salinity (although Salisbury et al, (2011) and Fournier et al. (2015) show how this can be used); on the other hand, the time averaging of the satellite products, in particular from L-Band, is often over one week or more, which is too long to display the detailed processes involved in the freshwater transport.

Pathways of freshwater transport have also been documented using data from surface drifters (Muller-Karger et al, 1988) and profiling floats (Hu et al, 2004), which illustrate large seasonal variability of the pathways. It is usually expected that in the early part of the year, the freshwater pathway along the Guiana shelves and into the Caribbean Sea is favoured.

These different studies have highlighted the importance of eddies in shaping where the transport of fresh shelf water to the deep ocean happens, in particular the anticyclonic eddies shed from the North Brazil Current retroflection near 8°N early in the year. These studies have also pointed out the sensitivity of the fresh water transport to wind magnitude and direction. Winds parallel to the coast and the shelf-break were found to be more favourable for offshore transport than wind perpendicular to the shore. Thus, during the early months of the year, when the atmospheric Inter-tropical Convergence Zone (ITCZ) shifts southward, the dominant northeasterly winds are not favourable for this off-shelf transport east of 53°W.

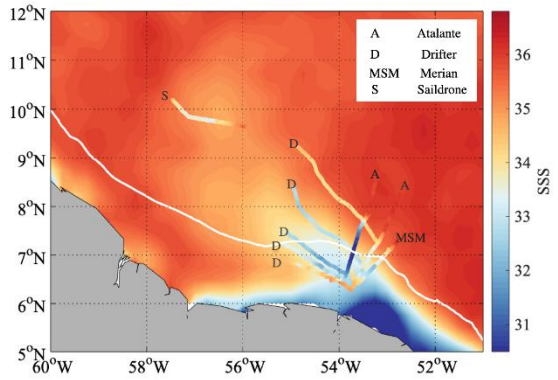

Figure 2: Average for February 2-19 2020 of the daily salinity fields based on SMOS and SMAP satellite data, overlaid with the data used in the fresh plume (A for R/V Atalante on February 2 and 5, MSM for R/V Maria.S.Merian on February 2; D for drifters on February 2 to 7 and S for saildrone on February 16-18). The different tracks/trajectories are colour-coded with salinity.

In early February 2020, during the Elucidating the Role of Clouds-Circulation Coupling in Climate Ocean-Atmosphere (EUREC^{4}A-OA) experiment (Stevens et al., 2021), the RV Atalante and the RV Maria S. Merian (MSM) surveyed an area close to the Guiana shelf just as a plume of freshwater was ejected from the shelf to the deep ocean (Fig. 2). Five instrumented drifters were deployed in this fresh water plume, which was also followed daily using satellite imagery (ocean colour and salinity from L-band radiometry), as well as model simulations (Mercator PSY2V4) and altimetry. An Uncrewed Surface Vehicle (USV) saildrone (Zhang et al, 2019) deployed for the EUREC^{4}A-ATOMIC (Atlantic Tradewind Ocean Mesoscale Interaction Campaign) cruises and equipped to measure sea surface temperature (SST), SSS, and current profiles is also used.

The period investigated in this paper spans from the 2nd to the 21st of February 2020, after which the fresh plume was less clear and there were less in situ or remote sensing data available.

2. Data

2.1 In situ data

Surface Velocity Program (SVP) drifters were instrumented by the company '*Pacific Gyre*' to measure temperature and salinity every 30 minutes at 20-cm, 5-m and 10-m depths. They also measured surface barometric pressure as well as wind speed and direction 0.5 m above the surface, with regular GPS positioning. Positions were edited for some erroneous data and are less certain for one drifter closer to the coast. Temperature and salinity data retrievals were good at 20-cm depth, with some early loss of data occurring at 5-m and 10-m depth. This was not an issue during the first 10 days of deployment except for one drifter not used here just to the north of the plume. For this investigation, the comparison of the three depth records does not suggest significant salinity biases.

A fleet of four USV saildrones operated in the eddy-rich area north of the Guianas (9-12°N) and crossed the freshwater plume during 17^{th}-18^{th} February. We use the position, temperature, salinity and wind reported every minute, as well as the ocean velocity profiles (300 kHz RDI Acoustic Doppler current profiler (ADCP)) averaged every 5 minutes from one NOAA saildrone. The velocity profiles from 6 m down to a maximum depth of 104 m are provided with a 2-m resolution.

Both RV Atalante and MSM continuously measured temperature and salinity from thermosalinographs pumping water near 5 m below the surface, and they measured wind from dedicated met-stations. During crossings of the fresh plume on the 2^{nd} and 4^{th}-5^{th} of February, either a moving vessel profiler (MVP) or a fast uCTD were deployed from RV Atalante, providing high resolution T-S profile sections across the plume in the upper 50 m. The RV

Atalante is also equipped with a 150 kHz RDI ADCP, providing currents 29 m below the sea surface. The MSM 75 kHz ADCP provides calibrated currents starting at 18 m below the sea surface (8-m bins).

In addition, on board MSM, the coherent on receive marine radar (MR) developed at the Helmholtz-Zentrum Geesthacht was operated for monitoring the surface roughness as well as the ocean surface currents in vicinity of the vessel. The MR operates at X-band (9.4 GHz) with a pulse repetition of 2 kHz with vertical polarization. The pulse length of 50 ns results in a range resolution of 7.5 m and the 7.5' antenna array allows an azimuthal resolution of 0.9°. The radar was operated with an antenna rotation frequency of ~0.45 Hz covering a range distance of 3.2 km around the vessel, thus a 6.4 km width along the track of the vessel. The normalized backscatter intensity results from the temporal mean radar backscatter intensity at every point, which is normalized and corrected for range and wind direction dependencies (Dankert and Horstmann, 2007). As the normalized backscatter intensity is strongly dependent on the ocean surface roughness it depicts all structures that affect the surface roughness. In addition, the MR image sequences are utilized to retrieve the near-surface current (approximately the upper 5 m currents) maps by analyzing the wave signal (Senet et al., 2001; Huang et al., 2016; Lund et al., 2018). Therefore, MR image sequence are converted from the spatio-temporal domain to the wavenumber-frequency domain via a 3D FFT. Within the wavenumber-frequency domain, the wave signal is located on the so-called dispersion shell. In the presence of a current, the Doppler effect leads to a translation and dilation of the dispersion shell. The current is determined using a fit that minimizes the wave signal's distance from the dispersion shell.

Between the two crossings of the plume, the two vessels surveyed a salinity-stratified area on the shelf. During this survey, the free-drifting platform Ocarina (Bourras et al, 2019) was deployed for a little more than 12 hours. This platform was equipped with a 1200 kHz ADCP to measure current profiles at 0.5 m resolution between 0.29 m and 17.29 m from the sea surface. These data are combined with temperature and salinity profiles collected from the RV Atalante MVP to estimate the gradient Richardson number (Ri) in this stratified near-surface layer at different times of the day.

2.2 Satellite data

The satellite data used are daily products of chlorophyll, mapped surface current from near-real time (NRT) DUACS-NRT altimetry products, and daily analyses of surface salinity based on a blend of data from different L-band radiometry satellite missions.

Daily chlorophyll-a (Chl*a*) concentration maps on a spatial grid of 0.02° are provided by CLS (https://datastore.cls.fr/catalogues/chlorophyll-high-resolution-daily). The maps are composites built from four satellite sensors, VIIRS (on Suomi-NPP and NOAA-20 US platforms) and OLCI (on Sentinel 3A and 3B Copernicus European platforms). The VIIRS L1A products are downloaded from the NASA Ocean Color Web, whereas the OLCI L1 products are downloaded from the EUMETSAT Copernicus On-line Data Access in NRT. As described in Stum et al. (2015), the Polymer software (Steinmetz et al, 2011) is used since 2014 to compute Chl*a* from the top of atmosphere reflectances. During our period of interest, they are usually without many gaps, except on the 13th to 17th of February. We use them qualitatively, so contamination by coloured dissolved matter or particles is not an issue for the objectives of this study. Geostrophic current maps are produced by Ssalto/Duacs and distributed by Copernicus-Marine Environment Services (CMEMS). The currents are

computed from absolute dynamical topography (ADT) mapped using an optimal interpolation method (Taburet et al, 2019). The maps (product SEALEVEL_GLO_PHY_L4_NRT_OBSERVATIONS_008_046) are produced daily on a 0.25°x 0.25° grid, based on combined altimetric data of all the satellite missions within the time window from at least 15 days before to 6 days after the date of interest. Mean currents are added to the anomaly as described in Rio et al. (2011). The spatial scales resolved in the currents are usually on the order of 100 km or more, with significant damping at smaller scales (see also Dibarboure et al, 2011, for an earlier product).

The salinity products used are level 2 (L2) fields of the Soil Moisture Ocean Salinity (SMOS, Jan. 2010-present), and Soil Moisture Active Passive (SMAP, Apr. 2015-present) missions. The European-led SMOS and the NASA-led SMAP missions observe the surface by L-band radiometry from sun-synchronous polar-orbiting satellites (Font et al, 2009; Kerr et al, 2010; Entekhabi et al, 2010; Piepmeier et al, 2017). Both SMOS and SMAP orbits cover the entire globe within 3 days with data provided close to 6 am and 6 pm local time. The retrieved SSS has a spatial resolution of ~45 km for SMOS and between ~40 and ~50 km for SMAP. Here, we use the SMOS L2Q fields (doi: 10.12770/12dba510-cd71-4d4f-9fc1-9cc027d128b0), corrected for systematic errors depending on the geometry of acquisition of the satellite (Boutin et al. 2018), delivered by Centre Aval de Traitement des Données (CATDS) and the SMAP L2 fields delivered by Remote Sensing System (RSS v4 40 km). The SMAP product is a little smoother than SMOS, and it generally has smaller errors also suggesting slightly larger scales resolved. Two SMOS images with evidence of Radio-frequency interference contamination have been removed during the period investigated, and the contamination became worse later in February. We also use SMOS and SMAP combined weekly SSS generated by the Climate Change Initiative Sea Surface Salinity (CCI+SSS) project

(doi:10.5285/4ce685bff631459fb2a30faa699f3fc5). It provides weekly SSS data from 2010 to 2019 at a spatial resolution of 50 km, a sampling of 25km and one day, by combining data from the SMOS, Aquarius and SMAP missions.

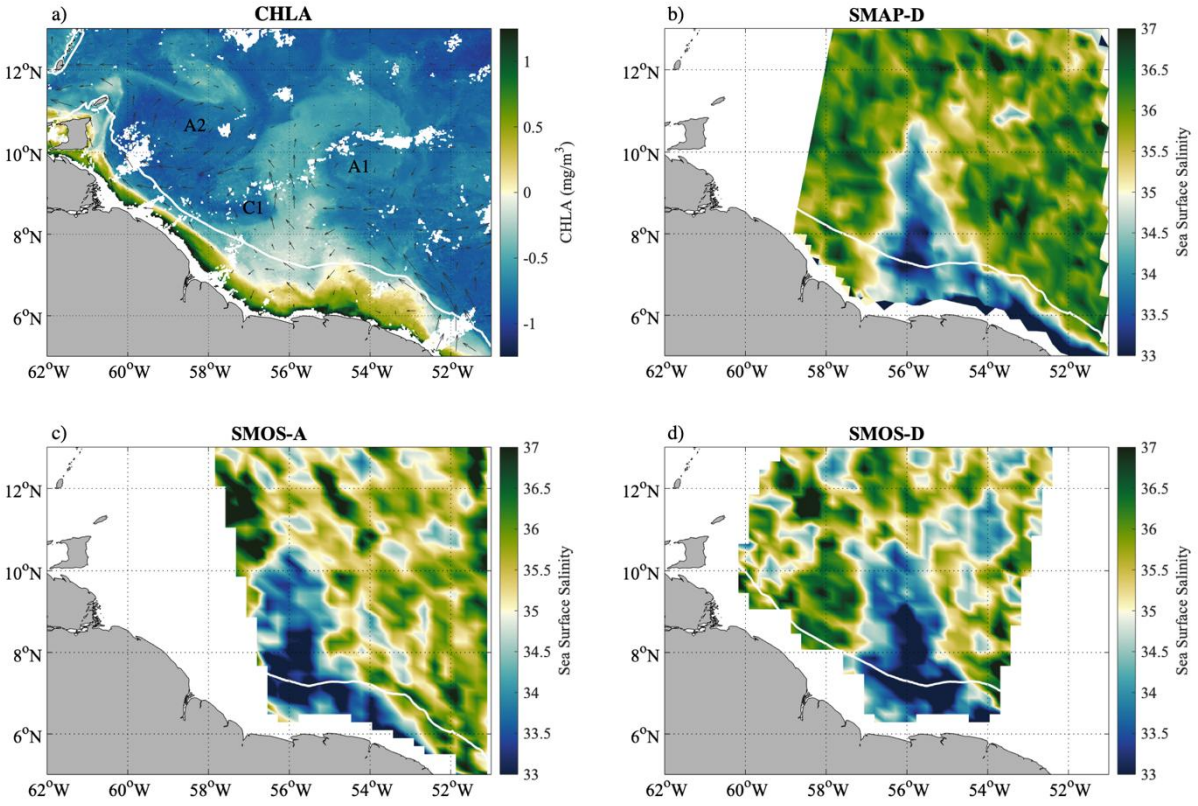

Figure 3: Satellite maps on February 12th. Chl*a* and geostrophic currents (grey arrows, a), SMAP SSS along its descending track (b), SMOS SSS along its ascending (c) and descending track (d) for the 12th of February. The shelf break is represented by the 100-m bathymetry contour (white line). Two anticyclonic (A1, A2) and one cyclonic (C1) eddy are labelled in (a).

We illustrate the different products on the 12th of February, when the fresh plume was fully developed along 56°W (Fig. 3). Both SMAP and SMOS SSS show a mostly south-to-north structure along 56°W extending from the shelf over to the deep ocean (shelf break in white), although with a slightly different pattern (note that they are taken 12 hours apart). The Chl*a* map also shows filaments and regions of higher load, which could be either chlorophyll, remnants of Colour Dissolved Organic Matter (CDOM) or remnants of sediment and detrital

matter not fully filtered out of the products. These structures align to some extent with the currents that connect the outer area of the shelf to the deep ocean. They are located on the western side of a large anticyclonic eddy shed by the North Brazil Current retroflection (A1). A smaller cyclonic structure (C1) is also visible close to the shelf break, southwest of the northward currents. The Chl*a* map presents finer scales, as expected from the better resolution of the satellite imagery in the visible part of the spectrum compared to L-band radiometry.

SMAP and SMOS L2 maps present systematic differences with respect to in situ data that also depend on whether they correspond to descending or ascending tracks. The issue is particularly large for the SMOS product where the systematic differences are also found to vary across the tracks, in particular on the eastern edge of the descending tracks due to a sun-tail contamination not filtered out in the L2Q fields. Part of this contamination is however detectable on the estimated error provided in the SMOS L2Q products and we eliminated SMOS data for which the estimated error was larger than 1 pss. We attempted to correct the remaining systematic differences on a track by track basis, although this is often uncertain at the 0.1 to 0.2 pss level, in particular for SMOS. We did not correct island effects on the SMAP maps that are particularly noticeable to the east/north-east of islands (Grodsky et al, 2018) because they are mostly outside of the main area of our study.

In order to provide full salinity fields and reduce errors by averaging enough data, we combined SMOS and SMAP L2 gridded fields. As the fresh plume evolves on a roughly daily time scale, as observed for example from Chl*a* maps, it is best to keep a rather short time averaging. For half the days, combining the tracks at 6 am and 6 pm (local time) was sufficient to provide a full coverage of the fresh water plume. For other days, it was necessary to add data from 6 pm of the previous day (thus a total time span exceeding 24 hours). This

leaves only two days with no salinity product, out of the 20 days investigated.

At each grid point, the field value is estimated by a simple weighting of data inversely proportional to the L2Q estimated error, and with a spatial weight decaying as a Gaussian with a radius of 30 km as a function of the distance of the data to the grid point. No data farther than 50 km is incorporated. We also assumed that errors on data closer than 25 km are fully correlated to account for the real footprint of the satellite data which is on the order of 50 km. The resolution of the final daily field is probably close to 70 km. Estimated uncertainties on the daily fields are typically on the order of 0.5 pss, consistent with the comparison to in situ data. These comparisons also suggest that the lowest salinities in the fresh plume often have been overestimated in these fields, with compensating underestimates on the sides of the plume. These are possible effects of the data smoothing, although we could not fully verify it as data coverage was not evenly distributed. These fields nevertheless give precious information on the fresh salinity distribution as illustrated on Fig. 2 for the average over 18 days.

The IFREMER CERSAT Global Blended Mean Wind Fields product, distributed by CMEMS, is used in this paper. It provides 6-hourly surface winds in the region of interest on a spatial grid of 0.25° in latitude and longitude. From 2010 to 2018 the reprocessed product is used (WIND_GLO_WIND_L4_REP_OBSERVATIONS_012_006), while for 2019 and 2020 we used the near real time one (WIND_GLO_WIND_L4_NRT_OBSERVATIONS_012_004).

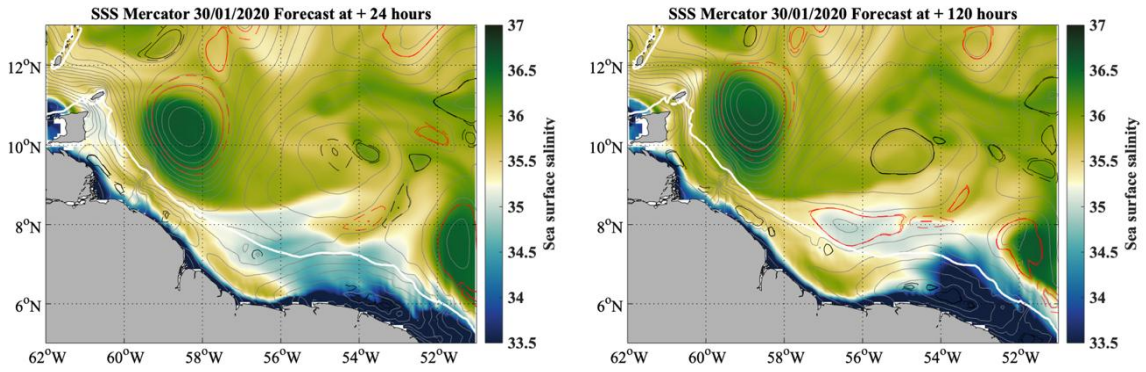

Fig. 4: Mercator SSS (colour) and sea level (grey contours) forecast and eddy detection made on the 30 Jan 2020 for 31 Jan 2020 (left) and 04 Feb 2020 (right). The eddy detection is shown by dashed contours (red for anticyclones and black for cyclones; Laxenaire et al, 2018). The shelf break is represented by the 100-m bathymetry contour (white line).

Finally, we used ocean velocity and salinity outputs from the Mercator model PSY2V4, both in analysis and forecast modes. These were made accessible, together with all satellite data to guide the ships during the field campaign in order to survey the fresh water plumes (Fig. 4). Since January 30th it consistently suggested a westward (and possibly offshore) extension of the eastern Guiana shelf fresh pool, although it sometimes missed the full extent of the plume's offshore extension.

3. Results

3.1 Life of the plume

In late January, the region located between 7°N north of the continental shelves of the Guianas and up to 12°N is mostly covered by surface water with a salinity between 35 and 36.5 pss, which is typical in this season of low precipitations and low input of freshwater from the Amazon and Orinoco rivers (Fig. 1). Freshwater is witnessed edging north-westward on the shelf east of French Guiana in late January, both in satellite products and in the Mercator simulations. Near 53°W, the shelf break bathymetry changes. Overall, the shallow isobaths tend to be zonally oriented west of 53°W, with a large cone (Demerara Rise) associated with

300 past sediment transport extending farther offshore and presenting less steep off-shelf
301 topography. Changes in geostrophic currents, often associated with the retroflection of the
302 NBC and formation of anticyclonic eddies to the northeast of the cone, would favour near-
303 surface northward transport. In addition, the wind direction being less orthogonal to
304 bathymetry would also favour off-shelf Ekman transport. Off-shelf transport events are thus
305 expected near that longitude.
306
307 Indeed, this is what was forecasted from the Mercator PSY2V4 operational model on January
308 30th with a clear off-shelf extension of the fresh pool indicated on February 4th, even though it
309 did not extend as a full-fledged plume (Fig. 4). Three SVP drifters were released into this
310 fresh plume on February 2nd, and two additional drifters were deployed during a return section
311 of RV Atalante on the 4th-5th of February a little further north, as the plume extended in that
312 direction (with salinity dropping across this section to close to 30 pss) (Fig. 2).

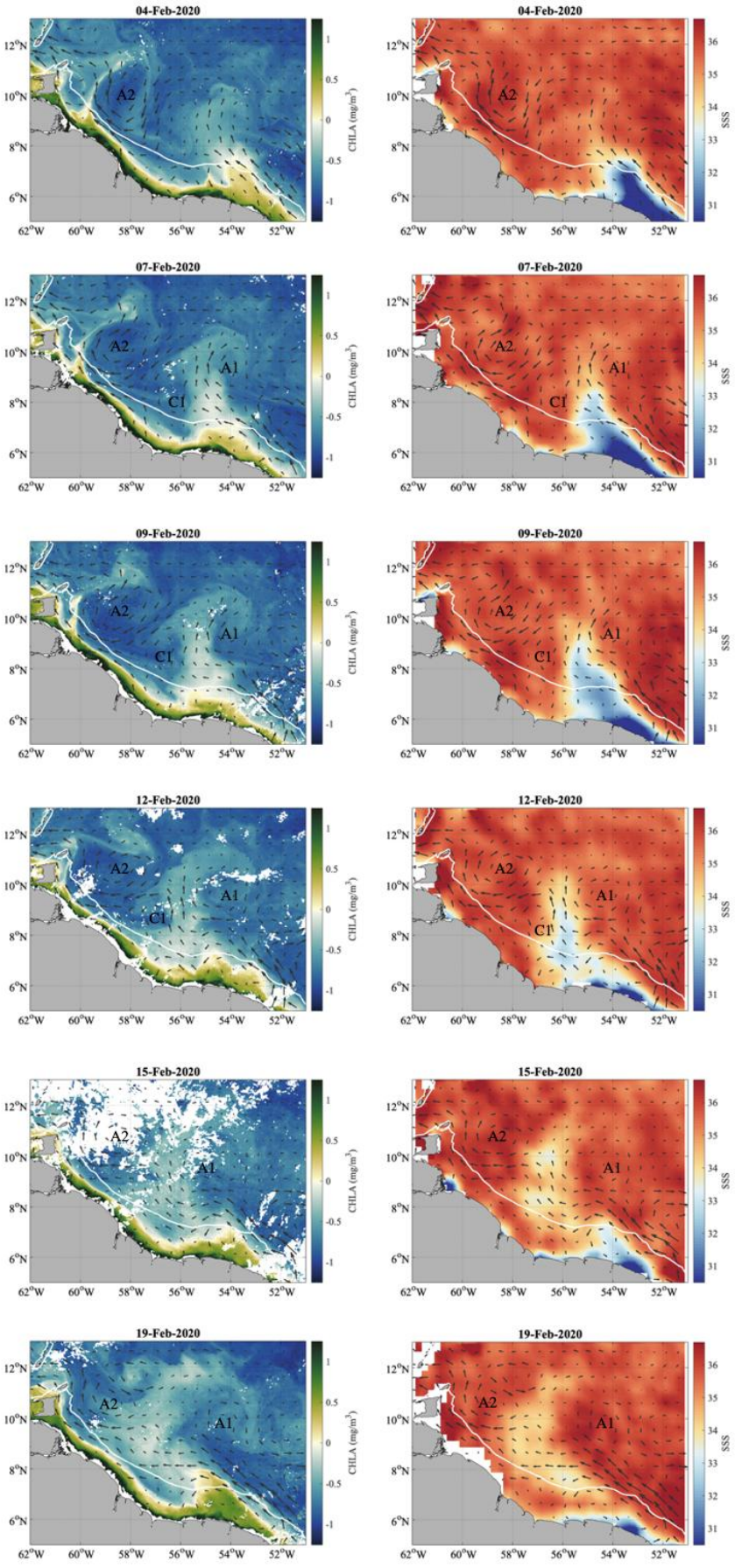
04-Feb-2020
04-Feb-2020
07-Feb-2020
07-Feb-2020
09-Feb-2020
09-Feb-2020
12-Feb-2020
12-Feb-2020
15-Feb-2020
15-Feb-2020
19-Feb-2020
19-Feb-2020
A1
A2
C1
CHLA (mg/m³)
SSS
12°N
10°N
8°N
6°N
62°W
60°W
58°W
56°W
54°W
52°W

313

Fig. 5: Snapshots of daily salinity and Chl*a* maps with overlaid geostrophic currents (grey arrows) for the 4th, 7th, 9th 12th, 15th and 19th of February 2020. The shelf break is represented by the 100-m bathymetry contour (white line).

To illustrate the plume evolution, we present (Fig. 5) daily snapshots of Chl*a* and surface salinity. The freshwater off-shore event started on February 4th, when the plume began to detach from the shelf, overflowing the shelf break near 53-54°W. An anticyclonic NBC ring (A1) northeast of the plume had already entrained relatively fresh water (SSS on the order of 35 pss) since late January all the way up to 10°N. This feature is also seen on the Chl*a* distribution across the shelf break. The northward offshore transport of fresh and productive water continued on the 7th of February, following fairly well the surface geostrophic currents. The anticyclonic eddy (A1) centred around 54.5°W-9.5°N likely participated in advecting water from the plume northward (on its western side) and limited its westward propagation. A small cyclonic eddy (56.5°W-8°N, C1) channelled the northward geostrophic flow and also contributed in steering the plume northward. The situation was quite similar on the 9th and on the 12th with the northernmost part of the plume, rich in chlorophyll, steered by the northern part of the anticyclonic eddy A1. In the meantime, the plume started to be influenced to its west by the eastern side of a second anticyclonic eddy (A2, centred around 58.5°W-11°N). Around the 12th, we observe the first indication (in particular in SSS) suggesting a future separation of the plume from the shelf. This separation started on the 14th of February and was clearly visible on the 15th. The dynamic situation changed quickly as the cyclonic eddy C1 disappeared, with a strong north-westward current near the shelf almost topographically steered, and the two anticyclones north of 9°N. The fresh pool formed by the plume spread horizontally (and probably vertically), with surface salinity on the order of 33.5-34 pss.

Intrusion of salty water from farther west near 9°N might have contributed to the erosion of

340 the salinity minimum. This is particularly pronounced on the February 15th map. At that date,
341 two drifters close together experienced very large salinity differences (up to 0.5 pss at 3-km
342 distance near 9°N/56.6°W), illustrating how sharp the gradients were near this wedge of salty
343 and low Chl*a* water. Horizontal mixing with the plume water can be expected from this date,
344 except if the saltier/Chl*a*-free water is entrained under the fresher water. This penetrating
345 saltier water seems to partially separate fresher water to the north from the freshwater closer
346 to the shelves.
347
348 On the 17th and 18th of February, the saildrone crossing the fresh pool still encountered SSS as
349 low as 33.3 pss near 9.8°N/56.5°W, similar to what is suggested by the salinity maps (Fig. 2
350 and Fig. 5). Then, by February 19th, the low salinity pool became less pronounced (minimum
351 values increase to 34 pss), but extended further westward. At places from 7°N to almost 12°N
352 its width reached up to 2° of longitude. Afterwards, it was difficult to follow because of the
353 uncertainties in the salinity maps that are on the order of 0.5 pss.

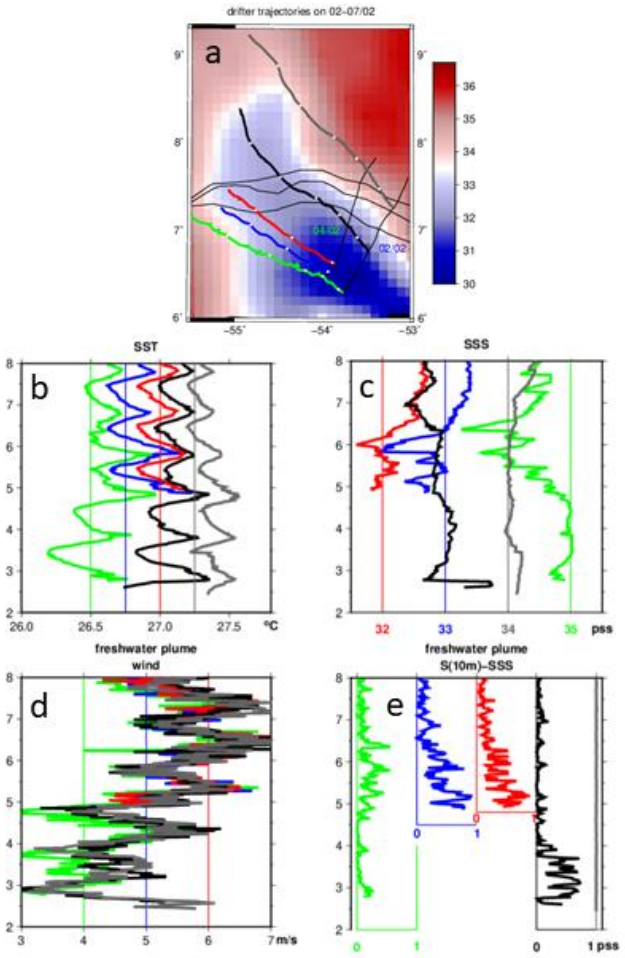

Figure 6: The drifter time series from February 2nd to 7th. Top panel, the trajectories (with dots each day at 0 GMT), as well as the SSS map for February 7. Below, four panels as a function of time (vertical axis in February days) for temperature (b, top left), salinity (c, top right), measured winds (d, bottom left in m/s), and salinity stratification S(10m)-S(0.2m) (e, lower right). The curves are colour-coded for the different drifters based on panel 6a (on 6e, the colored vertical straight lines correspond to no-stratification for that drifter).

Another way to investigate the plume evolution is to consider a Lagrangian perspective, based on the time series of the five drifters deployed in the plume (SSS lower than 35 pss) on February 2nd and 4th either on the shelf or near the shelf break. For the first four-five days after deployment they drifted north to north-westward and remained coherently separated cross-stream (Fig. 6a). The drifters are drogued at 15-m depth, which might be within the stratified layer under the freshest surface water, in particular at deployment (see section 3.2).

368 The drifters were deployed in a horizontal gradient of SST (1°C change across the plume),
369 with coldest water closest to the continent. Interestingly, this gradient as observed by the
370 drifters remained fairly consistent over time, although its amplitude gradually diminished
371 (Fig. 6b). Moreover, large temperature daily cycles are observed, with initial amplitude
372 exceeding 0.5°C. The wind (Fig. 6d) also illustrates a daily cycle with strongest wind in the
373 early morning and weakest wind in the late afternoon. It was relatively weaker at the
374 beginning of the deployment near the shelf break, in line with the corresponding larger
375 temperature daily cycle. For all drifters the wind increased over time during this initial five-
376 day period and as the drifters moved away from the shelf.
377
378 Salinity (Fig. 6c) variability between the different trajectories is not as regular as temperature
379 variability. The trajectories present some rather fast changes of SSS (by up to 1 pss), which
380 indicate the presence of small-scale gradients/blobs advected relative to the drifters. The red
381 salinity curve, corresponding to one of the middle deployments, remained the lowest.
382 Nevertheless, 7 days after its deployment, it has values very close to the black curve
383 (corresponding to a drifter located to its northeast, in slightly warmer water). It is the drifter
384 farthest east (grey line, always off shelf) which presents the least variability. All together
385 during this period and for all drifters, salinity is very similar at 0.20-m and 5-m depths
386 whereas there are gradients of up to 1 pss between the surface and 10 m for most drifters (Fig.
387 6e). This is not found for the drifter that is farthest from the shelf (grey curve). It indicates a
388 deeper fresh layer in this region, even though at times this drifter presents lower salinity than
389 the drifter closest to shore (green curve). The periods of large salinity stratification between
390 the surface and 10 m depth are not found at the same times for the different drifters (Fig. 6e).
391 They tend to be less common on February 6th and 7th, after a few days of drift away from the
392 shelf and with the stronger winds.

393

394 3.2 Sections across the plume (extension, gradients, thickness)

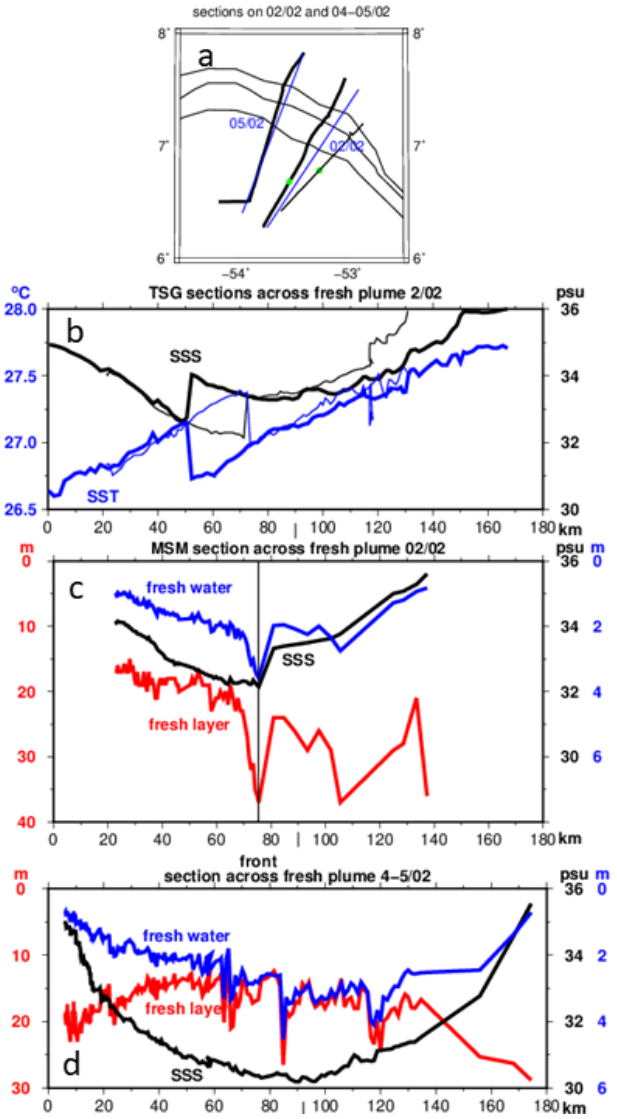

395

396 Figure 7: Sections across the shelf break near 53-54°W. (a) (top panel) Map with the different
397 sections (thick black line for RV Atalante on February 2nd, and 4th-5th and thin black line for
398 MSM on February 2nd). The blue lines indicate the axis along which the data are projected for
399 the plots (the 100-m, 300-m and 500-m isobaths are plotted), and the green dots the positions
400 of a T/S front. (b) SST (blue) and SSS (black) sections on 2nd of February from RV Atalante
401 (thick) and MSM (thin) transects. The horizontal axis is distance from the end point on the
402 shelf (53.72°W/6.27°N) and the data of the two ships are projected on the same line median to
403 the two ship tracks. (c) and (d) lower panels: the MVP section on 2/02 (MSM) and 4-5/02
404 (Atalante) plotted for SSS (black), fresh layer thickness (red) and freshwater thickness (blue),
405 with respect to distance from its origin on the shelf (starting at 75 km/134 km on the

406 first/second section, the MVP was replaced by a uCTD). The vertical bar on bottom axis on
407 both panels indicates the location of the 100-m isobath. For (c), the position of the sharp front
408 in SSS/SST is noted by a vertical line.
409
410 On the 2nd of February both RV Atalante and MSM crossed the nascent plume (Fig. 7a). The
411 overall currents were directed to the northwest, so in general the MSM section is upstream
412 from the Atalante sections. Both vessels were coming from the deep ocean over the outer
413 shelf, with salinity decreasing and reaching a plateau, until a sharp front was encountered by
414 the two ships. This front is located on the shelf near 53.51°W-6.68°N (Atalante) and
415 53.25°W-6.78°N (MSM), with much fresher (by more than 1.2 pss) and warmer water on the
416 inner-shelf side of the front (Fig. 7b; in the plots, the inner-shelf is to the left with values on
417 the x-axis increasing offshore). Interestingly, the front was farther away from the coast and
418 with warmer and fresher water on its southwest side for the MSM section compared to the
419 Atalante section (Fig. 7b). The surface front width is crossed in less than 100 m based on the
420 RV Atalante intake temperature sensor measurements, and is possibly as narrow as 50 m. The
421 respective positions of the front crossings by the two vessels suggest that the front was
422 oriented northeast to southwest. The lower SSS seen by MSM suggests that the front might
423 have been propagating from east to west, as fresher water was found farther upstream along
424 the shelf break and shelf (i.e., farther southeast) according to the salinity satellite maps and
425 Mercator model forecasts. Indeed, it is probably the same sharp front that was crossed by one
426 drifter (black line in Fig. 6c with more than 1 pss drop and 0.4°C warming in an hour) less
427 than 4 hours after its deployment from RV Atalante. As it is located a little to the north of the
428 position of the front crossed by RV Atalante, it suggests that the drifter was also encountering
429 freshwater coming from its east or southeast.
430
431 The MVP-uCTD section collected by MSM on February 2nd (note that the MVP started just

after crossing the surface front) will be summarized by presenting the thickness of the freshwater plume and total fresh water content (cf. salinity section in Supp. Inf. S4). The thickness of the freshwater plume (red curve in Fig. 7c) is defined here by the depth of the isohaline 0.5*(36.4 + SSS) corresponding to the depth where the fractions of surface and subsurface waters are equally mixed assuming homogeneous salinity profiles above and just below this depth and where 36.4 pss is a typical subsurface salinity near 50 m in this survey. The total fresh water content is estimated by vertically integrating the salinity profiles assuming mixing of fresh water with salty water at 36.4 pss. The thickness of the fresh layer and the total fresh water content (referred to 36.4 pss) present strong variability across the section (Fig. 7c). In particular, there is a large bulge in the freshwater layer thickness just inshore (left on Fig. 7c) from the front. Indeed, in this bulge, the very fresh surface water presents stratified salinity down from the near-surface to 40-m depth, with water properties at 22 m corresponding to those in the surface water that was crossed northeast of the front (cf. Supp. Inf. S4). This suggests that the freshest surface water had recently overlaid the saltier/warmer water, which had downwelled under the front. Farther to the northeast along that section, there is only a slight decrease of the fresh water content (blue curve on Fig. 7d) despite higher surface salinity (black curve on Fig. 7c, d), due to deeper surface mixed layer, especially east of the shelf break (but the number of profiles collected is insufficient to fully apprehend this structure).

On the 4th and 5th of February, RV Atalante crossed the fresh plume on its way from the shelf to the western side of the anticyclonic eddy A1 of Fig.3, a little bit to the west of the earlier crossings (Fig. 7a). Salinity dropped to nearly 30 pss close to the outer edge of the shelf (Fig. 7d) and presents very regular and symmetric along-track variability relative to the shelf edge, with no trace of the earlier fronts witnessed on February 2nd. This suggests that at that time the

plume was rather broad and at least 120 km across, assuming that the section was at a right angle to it. This assumption about the angle (maybe closer to 70°) is supported by the salinity maps, the drifter trajectories and the ship's vessel mounted ADCP (VM-ADCP), which suggest that the upper ocean currents were nearly at right angles to the cruise track.

The MVP (and uCTD) profiles provide information on the plume structure on February 5 (Fig. 7d). They indicate thicker fresh layers on the sides of the plume than in its middle, but shifted towards the shelf (red curve). The isohaline defining this layer thickness was typically found near 12 to 20-m depth, but the section presents also some very fast variability between successive profiles of the fresh layer thickness, for example at 65, 83, and near 120 km, which could be indicative of internal waves or solitons. There is no associated signature of the localised deep layers in surface salinity or temperature. The fresh water thickness is on the order of 2 to 4 m in the central part and outer part of the plume, whereas it decreases a little more towards the shelf edge of the plume.

3.3 Stratification and shear in the surface layer

The MVP sections performed close to the time when the plume separated from the shelf indicate that the fresh layer was rather shallow. We will present evidence of how this stratification constrains vertical mixing and the extent to which off-shore changes in the salinity plume are related to vertical mixing with the deeper saltier water.

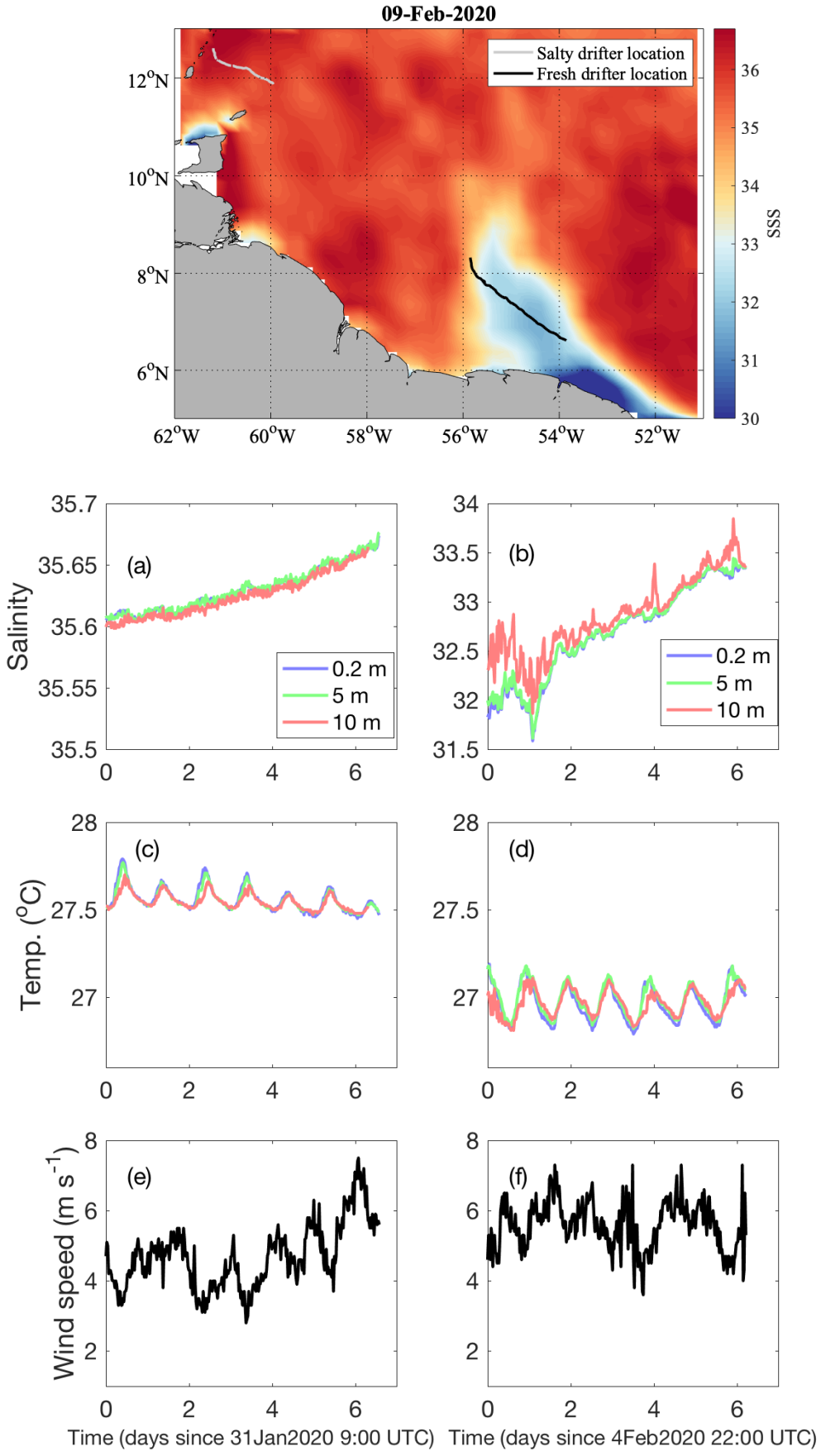

479

480

481 Figure 8: Salty (light grey) and fresh (dark) drifter trajectories are overlaid on the salinity map

for February 9 (g, top map). Under it, comparative time series for (left column) a drifter deployed in salty water (on Jan 31 at 09 GMT) and (right column) one in fresh water (on Feb 2 at 22 GMT). Top panels for temperature measurements at 0.2, 5 and 10m; middle panel for the salinity at these three levels, and bottom panel wind measurements.

The drifters show variable salinity stratification between the surface and 10-m depth in the first five days (Fig. 6e). Such stratification is less common afterwards, but some of the drifters also left the core of the fresh plume. Drifters launched in January, stayed out of the fresh water region and can be compared with those launched in the plume in order to identify the characteristics of this surface layer. Such an example is presented in Fig. 8, and although some differences might be related to weather conditions, such as different cloudiness, there are major differences between the drifter data in the plume and outside of the plume that we will comment. First, the temperature diurnal cycle is present in both the salty and fresh regions at the three depth levels but with strikingly different amplitudes (Fig. 8). The larger diurnal cycle is observed for the buoy located in the freshwater plume despite experiencing winds which were often larger than for the out-of-the-plume drifter. At night in the freshwater plume, temperature remains a little warmer at 10-m depth than at the surface. 10-m temperature however usually decreases during night-time, which suggests active night-time vertical mixing near the surface entraining the 10-m subsurface water. Furthermore, surface salinity increases similarly during day and night-time in the salty region, whereas the increase is observed with more diurnal variations in the fresh plume. Except for an event on the second day (Fig. 8), this seems to confirm the night entrainment of subsurface (salty) water into the near surface layer resulting in a late-night relative surface salinity maximum.

The records of the drifter data in the fresh plume therefore suggest night-time active mixing in the stratified layer near 10-m depth, just below the well-mixed surface layer. We do not have

direct information at that time of turbulence activity with the resolution needed. However, there is some indirect evidence provided by the Ocarina platform deployment over the shelf on February 3rd (Supp. Inf. S1). As the local depth was larger than 50 m, interaction of the surface mixed layer with the deep boundary layer should have been small. Nearby MVP profiles collected by RV Atalante are combined with the simultaneous Ocarina current data to estimate a Richardson number (Ri) profile (Supp. Inf. S1). This indicates values between 0.2 and 0.8 in the 6 to 16-m layer. As the profiles were not exactly simultaneous in space and time, we cannot estimate individual Ri profiles and derive precise statistics on the Ri distribution, although the average is on the order of 0.4. These averaged values suggest that the whole layer might have witnessed active turbulent conditions, with values close to the critical Ri for shear-induced instability (Galperin et al, 2007). This happened despite the stratification induced by daily heating, found at least between 6 and 14 m (15 m coincides with the lowest temperature in the profiles).

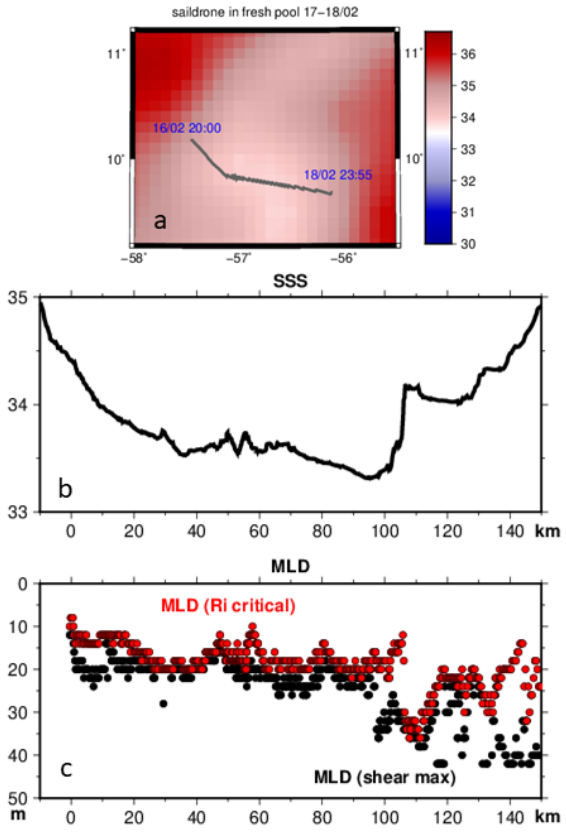

Figure 9: Saildrone section (16/02 evening to 18/02) across the fresh plume. (a) Track overlaid on the SSS map for February 17; (b) SSS; (c) different estimates of MLD (maximum shear depth in black and from critical Ri number in red). (b) and (c) are plotted along the section from west to east, as a function of distance from an entrance point in the fresh pool.

The saildrone crossed the fresh pool two weeks later than the ship on the 17^{th} and 18^{th} of February (Fig. 9a). They did not measure stratification directly, but the ADCP data at 2-m resolution can be used to estimate a mixing depth. It is done by assuming Ri=0.4 in this layer, where $Ri=-g/\rho *(d\rho/dz)/shear^2$. Thus, a density profile in the actively mixed layer is obtained by vertically integrating $Ri*shear^2 *\rho/g$ down from the surface. The bottom depth of this layer is reached when the density has increased relatively to the surface by 0.12 kg/m3 (Foltz et al. 2018). Alternatively, we use the current profiles to identify the depth of maximum shear. This depth is known to be deeper than the mixing depth, either because of internal waves under the base of the mixed layer or the wind momentum input into the surface layer (Foltz et al. 2020). The two estimates of the mixing depth are quite similar, with the one based on maximum shear being deeper by about 9 m on average. They are weakly correlated (0.42) over the crossing of waters with salinity less than 34 pss (Fig. 9b, c). That low correlation results from a small area near 100 km where the maximum shear is found deeper than the MLD based on critical Ri. Both estimates usually illustrate rather shallow mixing layers, often on the order of 20 m thick (averaging 17 m for the density criterion). The estimate is deeper in the eastern part after the sharp salinity frontal increase to 34.05 pss, where the two depths are closer to 30-40 m, which is more typical of what was found during the EUREC4A-OA surveys, at least at night time.

So, overall, the mixing layer depths (and presumably the freshwater layer thickness) in the plume are larger, possibly by close to 10 m, than what is observed on the sections two weeks

earlier and closer to the shelf. There is also no clear diurnal cycle of the mixed layer depth (MLD) within the plume, based on this indirect estimation (the freshest part of the plume was crossed in more than one day). This fits with the expectation that density stratification under sustained winds is constrained by the salinity stratification in these shallow and fresh surface layers. Interestingly, the width of the plume did not change much between February 2 (Fig. 6) and February 18. On the other hand, it expanded northward significantly based on the satellite maps (Fig. 4), extending to close to 12°N and becoming less linear. Minimum salinities reached in the plume are however larger by February 18.

3.4 Advective budget for the surface area.

To determine the causes of the freshwater plume's expansion, first we estimate the fresh water pool area from mapped satellite SSS daily products. We define it as the area bounded by the 35 pss isohaline and offshore of the 100 m isobath. We also estimate an advective area flux based on the currents across the shelf in sectors with salinity less than 35 pss. Currents are estimated by combining AVISO geostrophic currents and Ekman currents estimated with a mixing depth of 20 m and using wind stress estimates from the drifter closest to the shelf break. Note that 20 m is typical of the fresh layer thickness from the sections on the 2nd, 4th and 5th of February (Fig. 7c, d), but that is larger than the near 10-m MLD found on the southern part of those sections. It is also typical of the MLD observed by the saildrone section of February 17 (Fig. 9). The rate of change of the area should equal the area transport, assuming 2-D dynamics, no effect of mixing on this area, and conservation of SSS (no air-sea exchange of water).

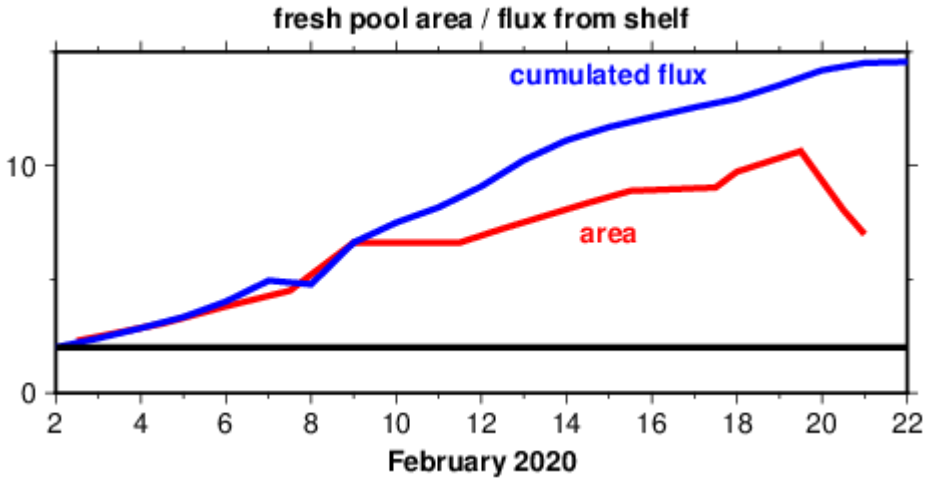

Figure 10: The area of the deep ocean sector with S < 35 pss and with depth larger than 100-m (in red; area expressed in 10^4 km^2); the cumulated flux is the horizontal area with S< 35 pss fed by advection from the shelf, estimated assuming horizontal dynamics, no mixing and conservation of surface salinity (in blue).

The two terms are comparable, although there is often a smaller area increase compared to the flux. The area of the freshwater plume increases rapidly from the 2nd to the 9th of February (Fig. 10) before increasing more slowly until the 19th and reaching a maximum of close to 100 000 km^2. Regarding fluxes, the increase is fast until the 14th of February and a bit slower until the 20th. As commented earlier on the plume history (section 3.1), starting on 13th-14th of February (Fig. 3), there are some signs of partial separation of the fresh water from the shelf (and thus, some plume discontinuity). Interestingly the total area transport was driven almost equally by Ekman and geostrophic advection until the 11th, and more by Ekman advection afterwards.

We have estimated the total freshwater transport based on ocean currents and the surface salinity maps, though this might be less precise compared to the area transport. We use a constant freshwater layer thickness of 20 m based on the initial sections (Fig. 7), and mixing with a 36.5 pss deep source. It indicates that the transport of fresh water in this off-shelf

plume averaged 0.15 Sv (10^6 m^3 s^{-1}) in the 11 days from February 2nd to 11th, and 0.6 Sv from the 11th to the 20th. During the first period, the transport is comparable to the expected outflow of the Amazon River in late January (based on climatology).

Until now, we have not commented on the uncertainties of these estimates. In Supp. Inf. S2, we estimate that uncertainties on the cumulative fluxes (blue curve on Fig. 10) are between 15% and 50% (depending on whether or not the error is random in the daily flux estimates), whereas the error on the total area is likely to be on the order of 10%.

Interpreting the difference between the two curves on Fig. 10 is therefore probably within the error bars. Some of the assumptions done for this budget might also break down. Vertical mixing might result in diminishing the area by bringing more salty water and thus the MLD salinity rising in some areas above the threshold (we found evidence of MLD deepening in the saildrone section on February 17th and 18th). There are also clearly some lateral intrusions/mixing with saltier water; how this affects the overall area is not straightforward. These issues will be more easily addressed in high resolution numerical simulations and a full three-dimensional budget, as the salinity fields clearly don't have the required resolution for these mesoscale or sub-meso scale features).

It is even more uncertain to provide an estimate of the total freshwater transport, as the freshwater thickness is not closely correlated to surface salinity, as illustrated in Fig. 7.

4. Discussion

4.1 Frequency of such freshwater plumes

How often do these freshwater events occur in the winter season during the January to mid-

March period, and what drives them? Using the 10 years of weekly CCI SSS products, in each year we find events of freshwater leaving the shelf and reaching the open ocean. Some events happened farther west, west of 56°W and in some cases the fresh water did not extend north of 10°N. These events (two thirds of the total) were unlikely to have a lasting influence in this sector of the Atlantic, with the freshwater being quickly washed across the Antilles into the Caribbean Sea. Events closer to the one observed in early February 2020 happened in 7 out of 10 years during the winter season (Supp. Inf. S3).

An important question is what determines the presence or absence of off-shelf transport. For that, a main requirement is a north-westward shelf transport of freshwater from near the equator to 7°N/54°W. At this place, the shelf-break direction changes and winds become less perpendicular to bathymetry and thus more prone to induce off-shelf transport. Southeast of that, the winds tend to be perpendicular to the shelf break, and even oriented a little farther anti-clockwise during that season. Therefore, close to the equator in this season, they often hinder the north-westward transport of freshwater on the shelf.

Thus, we considered the wind direction in 2020 and in the earlier years and defined an index based on the wind component parallel to the shelf-break at 3°N, which is a transition latitude with respect to the Coriolis force. It is halfway along the shelf between the Amazon estuary and French Guiana and is almost always bathed in freshwater. The index is the deviation of the wind component parallel to the shelf break from its average during the months of January and February of that year (positive to the northwest). In 2020, between mid-January to late February, we find only one four-day period (January 28-February 1) when the index is positive (Fig. 11). This change in wind direction would be favourable to a north-westward transport of freshwater which, if it propagates at 50 cm/s, would reach the shelf-break near

53-54°W in early February. The timing is thus fairly close to what is observed.

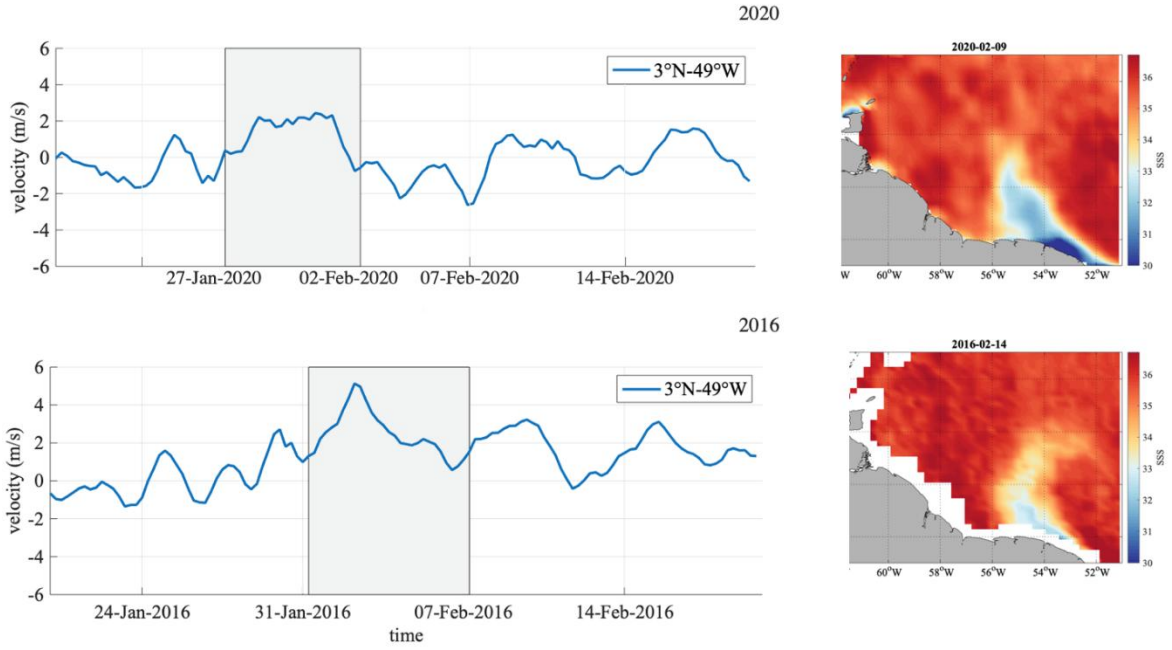

Figure 11: Winds at 3°N/49°W in relation to development of fresh plume events. Only the component of the wind parallel to 100-m isobath is shown on left side for two years (2020, the event we study here; and 2016, a typical other year), with the corresponding developed fresh plumes presented on the right side (for 2016, from CCI 7-day products). The grey time domain on the wind time series corresponds to the period between the start of the wind event and the start of the fresh plume separation from the shelf near 54-56°W.

We cannot carry out such a detailed calculation in other years, as we don't know the precise date of appearance of the plume. However, we find in 6 out of the 7 years when a fresh plume developed (the exception being 2018), a preceding period with significant positive wind index lasting for a few days. An example of that is presented in the lower panels of Fig. 11. The average length of these positive index events is 5.3 days (varying between 2 and 8.5 days), and the duration between the initial date of the wind event and the development of the fresh plume is 6.3 days (varying between 4 and 9 days). These estimates are in the range of what we expect for wind-induced currents. The time scales are long enough that geostrophy and Ekman divergence at the coast might be operating, which would reinforce the north-westward

geostrophic current. Of course, other dynamics such as those associated with the shelf-break currents, or the build-up of a pressure head and its evolution at the mouth of the Amazon estuary might also take place.

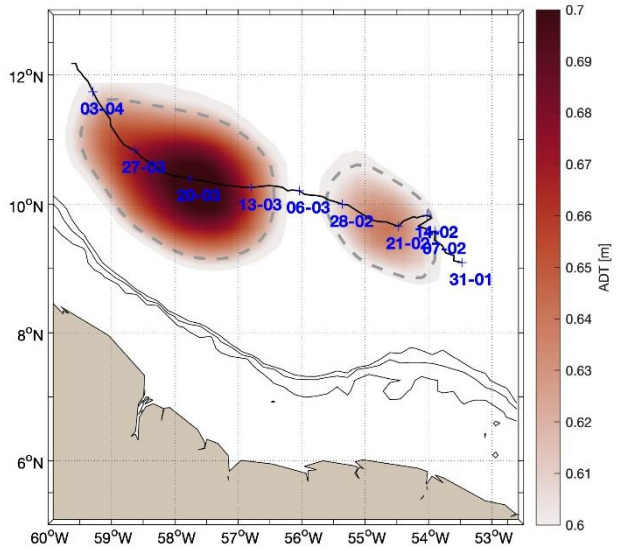

Figure 12: Trajectory of anticyclone A1 derived from ADT maps by the TOEddies algorithm (Laxenaire et al, 2018). Composite ADT signature of A1 are indicated for the Fe 23 and Mar 21. The shelf break is represented by the 100-m, 300-m and 500-m bathymetry contours (black lines).

Another key feature favouring the transport of the plume off the shelf is an anticyclonic eddy (A1) with a core lying slightly east of 54°W. This is actually a common area crossed by NBC rings. In 2020, the analysis of eddy A1 shows that it did not move very swiftly north-westward before February 21 (Fig. 12). In particular, between February 7 and 14, the core stalled and only marginally moved to the north, while separating from the shelf-break. This slow motion and the earlier presence of cyclonic feature C1 favours the channelling of the fresh plume by the geostrophic flow from the shelf-break farther north. At the same time, C1 weakens, and A2, another anticyclonic feature farther west slowly moves westward until mid-February, leaving a large area for the plume spreading. Then A1 rapidly moves farther west and intensifies, which would channel a large part of the fresh water closer to the shelf break

677 near Trinidad towards the Antilles (Fig. 12), as is suggested by the drifters and later weekly
678 salinity maps.
679
680 4.2 Sharp fronts
681 The daily salinity composite fields have a resolution on the order of 70 km, whereas the daily
682 composites for Chl*a* have a resolution slightly blurred by the compositing (for example a
683 feature moving at 30 cm/s will be displaced by 26 km in one day), and the geostrophic current
684 maps do not resolve structures with diameters smaller than 150 km, implying a large time
685 averaging. Much finer fronts are features common in the surveys (for example on Fig. 7 and
686 9). Some of these fronts have very large amplitudes, comparable to the mesoscales and are
687 associated with strong surface density changes, and thus are dynamically active. The best
688 resolved structure is the one crossed by two research vessels and one drifter on February 2nd
689 (Fig. 7). The intake temperature record of RV Atalante suggests a horizontal scale of the SST
690 and SSS front of less than 100 m and possibly as short as 50 m. According to the VM-ADCP
691 data of the two vessels, this surface front was embedded in a wider and deeper current
692 pointing north-westward. However, data also suggest a rather narrow surface velocity
693 structure just south of the front, with a sharp change of velocity at the sea surface front.
694
695 For instance, the RV Atalante absolute velocity presents a westward velocity peak of close to
696 30 cm/s at the front relative to the velocity before and after the front, despite the ship
697 navigating at a constant speed relative to the sea surface. This peak velocity lasts less than 3
698 minutes, thus over a rather small distance of less than 1 km. There is also some indication of a
699 change in the meridional velocity across the front, with the surface velocity is directed more
700 northward south of the front than north of the front. On MSM VM-ADCP shallowest bin at
701 18-m depth, the velocity vectors also suggest that the structure is converging at least in the

direction of the ship's track. There is also a westward narrow velocity peak of 25 cm/s over less than 7 km relative to velocities further away. However, because of the large salinity bulge southwest of the front (Fig. 7c) under the lowest surface salinity, these velocity structures at 18 m are difficult to interpret, as the bin is within the fresher layer close and southwest of the front, whereas it is in the saltier water under it in other areas. Fortunately, there is also the evidence from the MR radar surface data (Fig. 13)

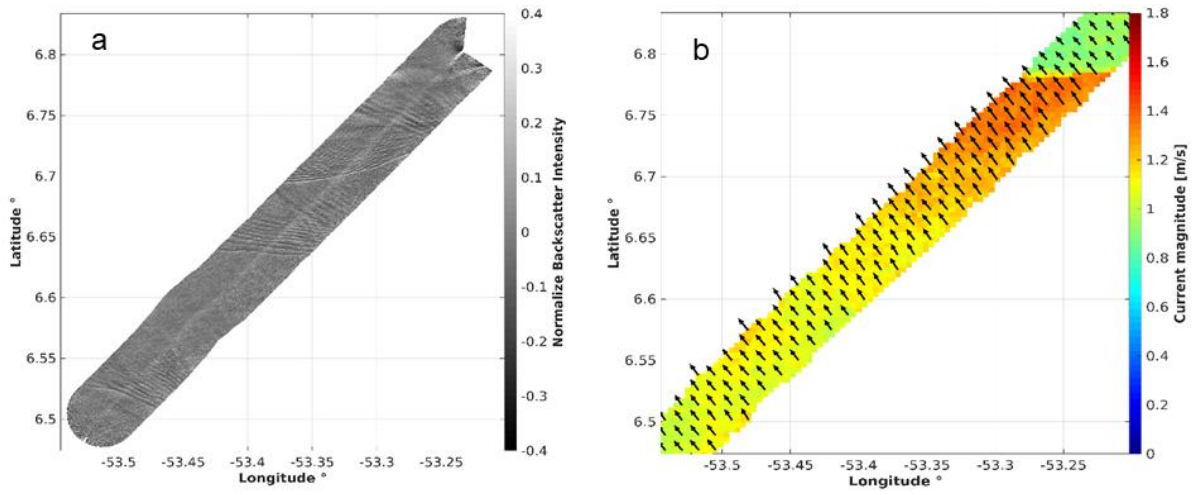

Figure 13: marine radar data between 14:03 and 17:42 on Feb 2 2020. Left panel show backscatter intensity, whereas right panel shows retrieved surface currents, both as arrows and colour-coded. The surface front was observed in T-S close to the north-east corner of the plots near -53.25°W/6.78°N.

As the normalized backscatter intensity is strongly dependent on the ocean surface roughness it depicts all structures that affect the surface roughness, including several internal wave packets are depicted along the track, as well as the strong current front close to the northeast corner of the plot. During the 3:39 h track plotted, the surface currents (top 5m) are pointing to the northwest with an increase of velocity along the track towards the northeast, until the velocity front is encountered at the same location as the SST/SSS front. The velocity front at

721 6.78°N is amost zonal with a slight southward tilt towards the west, and is associated with a
722 current gradient of approximately 0.5 m/s.

723

724 The drifter that crossed the front also shows a 50 cm/s westward velocity surge near the front.
725 This surge lasted over 2.5 hours, longer than the change in surface temperature and salinity
726 that lasted less than 1 hour. It is difficult to translate that into a horizontal scale of the current
727 feature, as it would involve knowing the velocity of the front relative to the drifter. Also,
728 notice that, according to the MSM section, the freshwater layer in the fresher part of the front
729 likely extended past the drogue depth centred at 15-m, so the drifter current represents a mix
730 of the velocity in the fresh surface layer and below it.

731

732 These different velocity estimates are in the same bulk range, and although the width of the
733 associated velocity structure is not the same between MSM and Atalante surface data, these
734 larger velocities in the 25-50 cm/s range close or just south of the front (near the freshwater
735 bulge) are close to the expected velocity of an internal gravity current assuming a Froude
736 number of 1 (with the change in stratification of a little over 1 pss and layer thickness of
737 ~20m). The velocity data suggest a front/gravity current propagating to the northwest or west
738 with respect to the underlying water at the time it was crossed. Such a propagating front
739 would quickly spread (by 20-40 km/day) the freshest shelf surface waters on top of the less
740 fresh waters found on the other side of the front, contributing to increased stratification of
741 salinity and density. Further investigation is required to better understand what sets this front
742 and its characteristics, and how it sheds internal waves, as is known to happen in other fresh
743 plumes (Nash and Moum, 2007).

744

745 4.3 Thickness of the fresh layer

746 The fresh layers appeared to have a shallow MLD even at night on February 5th, with a
747 stratified layer reaching to within 10 m of the surface. This stratification is also observed on
748 the earlier sections on February 2nd, and in the drifter data during the first five days after
749 deployment and as the fresh water starts separating from the shelf. However, the fresh layer is
750 thicker by 10-15 m or more in the MVP surveys just southwest of the surface front. These
751 different sections were positioned rather close to the north-westward edge of the fresh water
752 penetrating from the shelf, based on the daily SSS maps. This is also the case for the drifters,
753 with the salinity map in Fig. 6 for the last day of the trajectories on February 7th suggesting
754 close proximity of the drifters to the front. The mixing depth is somewhat deeper by February
755 17th-18th from the indirect estimate of the saildrone (at least 17 m), but with a large
756 uncertainty as density profiles were not measured. The difference between the two estimates
757 suggests that there has been some vertical mixing and entrainment of deeper saltier water into
758 the shallow surface fresh water during these 14 days. This is coherent with the velocity
759 profiles suggesting active turbulence in the fresh plume stratified salinity layer.
760
761 Such shallow layers also imply that the drogue of the SVP drifters, which is between 12 and
762 20-m depth, is only partially within the surface mixing layer, at least at their deployment in
763 the initial fresh plume. Their drift might thus differ from the speed of the freshest surface
764 water, possibly explaining why most drifters deployed in the fresh plume ultimately crossed
765 the salinity fronts to the west of the fresh plume (with Ekman veering, we expect the mixing
766 layer current to be to the right of the currents near its base). The observations from Ocarina on
767 the shelf in a salinity stratified layer (although much less stratified than in areas of lowest
768 surface salinity), also indicated a strong shear of the current within the top 17 m (close to 40
769 cm/s shear between depths of 1 m and 17 m). Such shear and shallow layer imply a strong
770 slippage of the surface layer relative to the layer just below, which could explain the fast

771 spreading to the north and north-west of the fresh water.

772

773 **5. Conclusions**

774 In early February 2020, in the core of the saltiest and driest period, a freshwater plume was
775 observed by satellite and in situ data entering the deep north-western tropical Atlantic near
776 54°W. This changes the perception that during this period, freshwater transport takes place
777 mainly on the shelf and close to the shelf break. This plume was initially very surface trapped
778 with stratification up to 10-m depth and with a width on the order of 120 km. Its freshwater
779 content corresponded of 2 to 3 meters of Amazon water and was distributed down to 40 m,
780 although most of its water is found in the top 20 m. The off-shelf transport lasted for at least
781 10 days with freshwater transport comparable to the Amazon outflow in January. The plume
782 was still quite well defined 16 days after it started spreading off the shelf break to reach a
783 maximum area of 100000 km^2, and up to 400 km further north. At this time, the mixed layer
784 had not deepened to more than 20 m as indicated by current profiler data during a saildrone
785 transect. Of course, this is hard to put into context from the limited *in situ* data, but the mixed
786 layer was shallower than night-time mixed layers found nearby in saltier waters. A slight
787 change in wind direction along the shelf between the Amazon estuary and 6°N for more than
788 3 days in late January seems to have triggered the north-westward flow of Amazon freshwater
789 along the shelf and towards the shelf break. The off-shelf plume was steered by eddies, and in
790 particular by a nearly-stationary anti-cyclonic North Brazil Current ring up to 12°N. It also
791 spread towards the Caribbean, due to the evolution of the different mesoscale eddies and to
792 the Ekman transport.

793

794 The presence of such events of freshwater transport in February is documented since 2010 in
795 7 out of 10 years, where changes in wind direction closer to the equator concomitant to the

presence of anticyclonic eddies to the east of the plume separation from the shelf seems to have contributed to their development and evolution. Such events should contribute largely to freshening the surface salinity in February or March north of the Guiana shelves and south of 12°N. It seems that the mechanism at work here is rather different than what was commented for anomalies later in the year leading to boreal summer, where both current anomalies, wind anomalies, interannual anomalies of Amazon outflow, or conditions upstream south of the equator seem to play important roles.

The position of the 2020 plume's first offshore extension near 54°W is east compared to the other plumes detected in CCI products for the other years. We found that such plumes in February are not rare, and are also commonly associated with NBC rings such as A1 that was nearly stationary during the plume development. This near stationarity could be linked with the presence of the Demerara Rise to its west that might act to trap the eddy and prevent its fast westward propagation. Clearly more research on the frequency of this phenomenon and how it is modulated seasonally and interannually will be interesting. Also, from the CCI weekly salinity maps, this also seems to happen in March, and maybe early April, though this will require further investigation. Afterwards in the spring season, with the seasonal wind changes and large Amazon outflow, it is however likely that other processes involved in the development of interannual salinity anomalies in this region east of the lesser Antilles and north of the Guiana shelves might dominate.

Acknowledgments

This work is a contribution to the LEFE/IMAGO-GMMC project EUREC^{4}A-OA, to the JPI-Ocean project EUREC^{4}A-OA, and to the TOSCA SMOS-Ocean project supported by CNES (Centre National d'Etudes Spatiales). LO was supported by a scholarship from ENS and

Sorbonne Université. Support for the salinity drifters was provided by the Climate Variability and Predictability Program of NOAA's Climate Program Office. GRF was supported by base funds to NOAA/AOML's Physical Oceanography Division. DZ was supported by NOAA's Climate Program Office, Climate Variability and Predictability Program. We benefited from numerous data sets made freely available and listed here : the SLA and currents produced by Ssalto/Duacs distributed by the CMEMS (https://resources.marine.copernicus.eu), the Chl*a* maps produced by CLS, the SMOS L2Q maps produced by CATDS (CATDS, 2019) and the SMAP maps produced by Remote Sensing System and CCI+SSS maps produced in the frame of ESA CCI+SSS project.

References

Boutin, J., Vergely, J.-L., Marchand, S., d'Amico, F., Hasson, A., Kolodziejczyk, N., et al. (2018), New SMOS Sea Surface Salinity with reduced systematic errors and improved variability. *Remote Sensing of Environment, 214*, 115–134.

Bourras D., Cambra R., Marié L., Bouin M.N., Baggio L., Branger H., Beghoura G., Reverdin G., Dewitte Boris, Paulmier Aurélien, Maes Christophe, Ardhuin F., Pairaud I., Fraunié P., Luneau C., Hauser D. (2019), Air-sea turbulent fluxes from a wave-following paltform during six experiments at sea. *J. Geophys. Res. Oceans*, *124* (6), 4290-4321. ISSN 2169-9275.

CATDS (2019). CATDS-PDC L3OS 2Q - Debiased daily valid ocean salinity values product from SMOS satellite. CATDS (CNES, IFREMER, LOCEAN, ACRI). https://doi.org/10.12770/12dba510-cd71-4d4f-9fc1-9cc027d128b0

Dankert, H., & Horstmann, J. (2007), A marine radar wind sensor. *J. Atmosph. Ocean. Technol., 24* (9), 1629-1642.

Dibarboure G., Pujol M.-I., Briol F., Le Traon P.-Y., Larnicol G., Picot N., Mertz F., &Ablain M. (2011), Jason-2 in DUACS: first tandem results and impact on processing and products. *Marine Geodesy Jason-2 Special Issue, 2* (34), 214-241.

847 Entekhabi, D., Njoku, E. G., O'Neill, P. E., Kellogg, K. H., Crow, W. T., Edelstein, W. N., et
848 al. (2010), The soil moisture active passive (SMAP) mission. *Proceedings of the IEEE, 98*(5),
849 704–716.
850 Foltz, G. R., Hummels, R., Dengler, M., Perez, R. C., & Araujo, M. (2020), Vertical
851 turbulent cooling of the mixed layer in the Atlantic ITCZ and trade wind regions. *J. Geophys.*
852 *Res., 125*, e2019JC015529, doi:10.1029/2019JC015529.
853 Foltz, G. R., Schmid, C., & Lumpkin, R. (2018), An enhanced PIRATA data set for tropical
854 Atlantic ocean-atmosphere research. *J. Climate, 31*, 1499-1524, doi:10.1175/JCLI-D-16-
855 0816.1.
856 Foltz, G. R., Schmid, C., & Lumpkin, R. (2015), Transport of surface freshwater from the
857 equatorial to the subtropical North Atlantic Ocean. *J. Phys. Oceanogr., 45*, 1086-1102,
858 doi:10.1175/JPO-D-14-0189.1.
859 Font, J., Camps, A., Borges, A., Martín-Neira, M., Boutin, J., Reul, N., et al. (2009), SMOS:
860 The challenging sea surface salinity measurement from space. *Proceedings of the IEEE,*
861 *98*(5), 649–665.
862 Fournier, S., Chapron, B.,Salisbury, J., Vandermark, D., & Reul, N. (2015), Comparison of
863 spaceborne measurements of sea surface salinity and colored detrital matter in the Amazon
864 plume. *J. Geophys. Res., 120*, 3177-3192.
865 Fournier, S., Vandermark, D., Gaultier, L., Lee, T., Jonsson, B., & Gierach, M.M. (2017),
866 Interannual variation in offshore advection of Amazon-Orinoco plume water: observations,
867 forcing mechanisms, and impacts. *J. Geophys. Res., 122*, 8966-8982.
868 Galperin, B., Sukoriansky, S., Anderson, P.S. (2007), On the critical Richardson number in
869 stably stratified turbulence. *Atmos. Sci. Let., 8*, 65-69, https://doi.org/10.1002/asl.153

Grodsky, S. A., Reverdin, G., Carton, J. A., & Coles, V. J. (2014), Year-to- year salinity changes in the Amazon plume: Contrasting 2011 and 2012 Aquarius/SACD and SMOS satellite data. *Remote Sens. Environ*., *140*, 14–22, doi:10.1016/j.rse.2013.08.033.

Grodsky, S. A., Vandermark, D. & Feng, H. (2018), Assessing coastal SMAP surface salinity accuracy and its application to monitoring Gulf of Maine circulation dynamics. *Remote Sens.*, *10*(8), https://doi.org/10.3390/rs10081232

Hu, C., Montgomery, E. T., Schmitt, R. W., & Muller-Karger, F.E. (2004), The dispersal of the Amazon and Orinoco River water in the tropical Atlantic and Caribbean Sea: Observation from space and S. PALACE floats. *Deep-Sea Res. II*, *51*, 1151-1171, https://doi.org/10.1016/j.dsr2.2004.04.001.

Huang, W., Carrasco, R., Shen, C., Gill, E.W., & Horstmann, J. (2016), Surface current measurements using X-band marine radar with vertical polarization. *IEEE Trans. Geosci. Rem. Sens., 54* (5), 2988-2997.

Kerr, Y. H., Waldteufel, P., Wigneron, J.-P., Delwart, S., Cabot, F., Boutin, J., et al. (2010), The SMOS mission: New tool for monitoring key elements of the global water cycle. *Proceedings of the IEEE*, *98*(5), 666–687.

Laxenaire, R., Speich, S., Blanke, B., Chaigneau, A., & Pegliasco, C. (2018), Anticyclonic eddies connecting the western boundaries of Indian and Atlantic oceans. *J. Geophys. Res. Oceans*, *123* (11), 7651-7677, doi:10.1029/2018JC014270.

Lund, B., Haus, B. K., Horstmann, J., Graber, H. C., Carrasco, R., Laxague, J. M., Novelli, G., Guigand, C. M., Özgökmen, T. M. (2018), Near-surface current mapping by shipboard marine X-band radar: A validation. *J. Atmos. Oceanic Technol., 35* (5), 1077-1090, doi:10.1175/jtech-d-17-0154.1

Mignot, J., Lazar, A., & Lacarra, M. (2012), On the formation of barrier layers and associated vertical temperature inversions: a focus on the northwestern tropical Atlantic. *J. Geophys. Res*., *117*, C02010, doi:10.1029/2011JC007435.

Muller-Karger, F.E., Mc Lain, C.R., &Richardson, P.L. (1988), The dispersal of the Amazon's water. *Nature*, *333*, 56-58.

Nash, J. D., & Moum, J.M. (2005), River plumes as a source of large- amplitude internal waves in the coastal ocean, *Nature*, 437, 400– 403.

Piepmeier, J. R., Focardi, P., Horgan, K. A., Knuble, J., Ehsan, N., Lucey, J., et al. (2017), SMAP L-band microwave radiometer: Instrument design and first year on orbit. *IEEE Trans. Geosci. Rem. Sens.*, *55*(4), 1954–1966.

Reul, N, Grodsky, S. A., Arias, M., Boutin, J., Catany, R., Chapron, B., et al. (2020), Sea surface salinity estimates from spaceborne L-band radiometers: An overview of the first decade of observation (2010–2019). *Remote Sensing of Environment*, *242*, 111769.

Rio M. H., Guinehut, S., and Larnicol, G. (2011), New CNES CLS09 global mean dynamic topography computed from the combination of GRACE data, altimetry, and in-situ measurements, *J. Geophys. Res*., 116, C07018, https://doi.org/10.1029/2010JC006505.

Salisbury J., Vandemark, D., Campbell, J., Hunt, C., Wisser, D., & Reul, N. (2011), Spatial and temporal coherence between Amazon River discharge, salinity, and light absorption by colored organic carbon in western tropical Atlantic surface waters. *J. Geophys. Res. Oceans* , *116*(C00H02), 14 p. Publisher's official version : https://doi.org/10.1029/2011JC006989 , Open Access version : https://archimer.ifremer.fr/doc/00041/15218/

Senet, C.M., Seemann, J., & Ziemer, F. (2001), The near-surface current velocity determined from image sequences of the sea surface. *IEEE Trans. Geosci. Rem. Sens.*, *39* (3), 492-505.

Steinmetz, F., Deschamps, P.Y, &. Ramon, D. (2011), Atmospheric correction in presence of sun glint: application to MERIS. *Optics Express*, *19*(10), 9783-9800.

Stevens, B., et al. (2021), EUREC^{4}A. Submitted to Advances in meteorology.

Stum, J., Tebri, H., Lehodey, P., Senina, I., Greiner, E., Lucas, M., & Steinmetz, F. (2015), NRT operational chlorophyll maps for marine applications. Poster presented at the 2nd IOCS meeting, San Francisco, June 15-18, 2015. Available at http://www.eposters.net/pdfs/nrt-operational-chlorophyll-maps-calculation-for-marine-applications.pdf

Taburet, G., Sanchez-Roman, A., Ballarotta, M., Pujol, M. I., Legeais, J.-F. Fournier, F., Faugere, Y., & Dibarboure, G. (2019). DUACS DT2018: 25 years of reprocessed sea level altimetry products. *Ocean Sci*., *15*, 1207–1224, https://doi.org/10.5194/os-15-1207-2019.

Zhang D, Cronin, M.F., Meinig, C., Farrar, J.T., Jenkins, R., Peacock, D., Keene, J., Sutton, A., & Yang, Q. (2019), Comparing Air-sea flux measurements from a new unmanned surface vehicle and proven platforms during the SPURS-2 Field Campaign. *Oceanography*, *32*(2):122-133.